IEEE Access
Multidisciplinary ⋮ Rapid Review ⋮ Open Access Journal

Received 26 May 2023, accepted 5 June 2023, date of publication 7 June 2023, date of current version 20 June 2023.

Digital Object Identifier 10.1109/ACCESS.2023.3283917

RESEARCH ARTICLE

Surface Wave, Skin Effect, and Per Unit Length Parameters of the Single-Wire Transmission Line at Low Frequency, for Nonmagnetic and Magnetic Wires

JOSÉ A. BRANDÃO FARIA[1], (Life Fellow, IEEE), RODOLFO ARANEO[2], (Senior Member, IEEE), AND ERIKA STRACQUALURSI[2], (Member, IEEE)

[1]Instituto de Telecomunicações, Instituto Superior Técnico, Universidade de Lisboa, 1049-001 Lisbon, Portugal
[2]Department of Astronautical, Electrical and Energy Engineering, University of Rome "La Sapienza", 00184 Rome, Italy

Corresponding author: José A. Brandão Faria (brandao.faria@tecnico.ulisboa.pt)

This work was supported by the FCT/MCTES through national funds and when applicable co-funded by European Union (EU) funds under Project UIDB/50008/2020.

ABSTRACT Surface wave technology for high-speed communications is a current research topic aimed to respond to increasing data rate demands on existing copper infrastructures. Also, the topic of surface waves has recently gained importance in the modeling of transmission line towers hit by lightning strikes with spectral content in the megahertz band. The single-wire transmission line structure (return conductor absent) cannot support TEM waves; it supports a TM Sommerfeld wave fully described by two propagation constants and two characteristic impedances. Nonetheless, the literature on single-wire transmission-line structures has been employing quasi-static per unit length constitutive parameters, inductance and capacitance, borrowed from ordinary two-conductor transmission line TEM analysis. This work develops, discusses, and compares various possible definitions of these constitutive parameters using different physical approaches: TEM-approach, circuit-approach, and energy-approach. Numerical results for nonmagnetic and magnetic wires, copper and steel wires, respectively, are obtained in the range 1 Hz to 1 GHz. Our analysis shows that in some circumstances the TEM and circuit approaches may lead to nonphysical results, but, remarkably, all the approaches seem to converge to a common dominant term either in the per unit length capacitance or in the per unit length inductance, whose product is frequency-invariant. Considering the different approaches under discussion, the differences among the observed results for the per unit length constitutive parameters are negligibly small, of second-order importance.

INDEX TERMS Magnetic wires, per unit length parameters, single wire transmission line, skin effect, Sommerfeld wave, surface waves, transmission lines, transmission line towers.

I. INTRODUCTION

The subject of surface waves —electromagnetic waves guided by and along the boundary surface between two different media— gave its first steps at the turn of the 20th century pioneered by Sommerfeld [1], [2], followed by Zenneck [3], and Goubau [4], [5], [6]. While Zenneck waves propagate along a planar boundary surface, Sommerfeld and Goubau waves develop along cylindrical surfaces, namely metal wires, bare or dielectric coated, respectively.

With broadband properties, the Sommerfeld wave, guided by an indefinitely long current-carrying lossy bare wire, does not radiate; it propagates axially at subluminal velocity with very low attenuation. Outside the wire, the wave's unbounded

The associate editor coordinating the review of this manuscript and approving it for publication was Alon Kuperman.

electromagnetic field is described by Hankel functions. Far away from the wire, the fields decrease exponentially with the radial distance, but near the wire they practically follow a simple inverse distance law, meaning that Sommerfeld waves are loosely confined around the wire, [7].

Wave confinement concerns, together with wave launching problems, delayed the fast development of surface wave applications in those early days. Nonetheless, it was well-known that the lateral spread of the field around the wire would diminish with the frequency. Therefore, without surprise, subsequent technological applications of surface waves have considered increasingly higher frequencies: from microwaves to terahertz and beyond, to optics and photonics, where the subject of surface plasmon-polaritons has become a vibrant research field [8].

With regard to "low" frequency phenomena, up to the UHF band, surface wave applications are also making their way, receiving more and more attention. For example, exploring new channels for high-speed communications on existing wiring infrastructures [9], [10], [11], [12], [13], [14]; improving the mid-range wireless transfer problem [15], [16]; modeling overhead power lines in high-frequency regions [17], and modeling power line towers struck by lightning [18], [19]. In this context, several papers addressing surface wave problems have referred to or dealt with the concept of per-unit-length capacitance and inductance parameters [12], [20], [21], [22], targeting an alternative circuit-type description of surface wave propagation phenomena.

In the framework of TEM or quasi-TEM propagation, the meaning of the per-unit-length (pul) parameters for transmission lines with two or more wires is sound and well-known [23], [24]. However, for the single-wire transmission line (SWTL), where the return current is not supported by a return wire, the use of pul parameters is somehow perplexing [20], [25], [26].

Devoted to the SWTL structure, the focus of this article is also set on the low frequency range, 1 Hz – 1 GHz, where Hankel functions have small argument and Sommerfeld wave parameters (propagation constants and characteristic wave impedance) can be accurately evaluated using solely the information conveyed by the skin effect impedance of the wire calculated from ordinary skin effect theory.

The main purpose of this work is the computation, analysis, and discussion of the usage of pul parameters to model the SWTL structure. The novelty stands on the fact that this is achieved by considering various approaches with different physical perspectives —TEM approach, circuit approach, and energy approach.

The analysis and discussion of the pul parameters begins with the ordinary case of a copper wire. Afterwards, we add a novel contribution, considering the case of a wire made of carbon steel (the building material of power line towers). Carbon steel is a good conductor with magnetic properties that dissipates energy through two mechanisms, Joule losses and magnetization losses; the first is taken into account via the wire's electric conductivity, the second via the imaginary part of the wire's magnetic permeability. The peculiar frequency behavior of the skin effect impedance exhibited by the magnetic wire leads to radial and axial components of the Sommerfeld wave quite different from those observed in the copper wire case.

Readers interested in an historic perspective and future developments of surface waves may refer to [14] and [27].

This work is organized into seven sections, the first of which is introductory. Section II presents a summary of the frequency-domain field equations of the Sommerfeld wave (principal TM mode), including the definition of radial and axial propagation constants. Energy flow perpendicular and parallel to the wire is discussed in Section III. A simple procedure useful for relating wave parameters and skin effect at frequencies where the Hankel functions have small argument is proposed in Section IV. Considering diverse physical perspectives, the concepts of pul capacitance and pul inductance in single wire transmission lines are worked out in Section V. The presentation and discussion of computation results, for nonmagnetic and magnetic wires, occupies the Section VI. Devoted to conclusions Section VII ends the article.

II. FREQUENCY DOMAIN FIELD EQUATIONS

Consider a single-wire transmission line consisting of a current-carrying cylindrical metal wire of radius a immersed in free space (ε_0, μ_0, $c = 1/\sqrt{\varepsilon_0\mu_0}$, $\beta_0 = \omega/c$) —see Fig. 1.

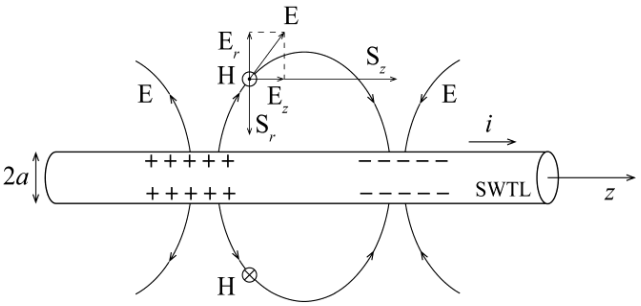

FIGURE 1. Longitudinal view of the circular cylindrical single-wire transmission line (SWTL): Geometry, electromagnetic field components and Poynting vector components.

With assumed linear behavior, the wire is generically characterized by two complex frequency-dependent constitutive parameters, the permittivity ε_w and the permeability μ_w.

The intensity i of the total current flowing in the wire, propagating along z, is time-harmonic of frequency ω, given by:

$$\begin{cases} i(z,t) = Ie^{-\alpha z}\cos(\omega t - \beta z) = \mathrm{Re}\left(Ie^{-\gamma z}e^{j\omega t}\right) \\ \gamma = \alpha(\omega) + j\beta(\omega) \end{cases} \tag{1}$$

where $Ie^{-\gamma z}$ is the phasor of $i(t)$ at generic z, and γ is the axial complex propagation constant. The positive real frequency-dependent quantities α and β are the attenuation and phase constants, respectively.

The presence of a z-directed current implies the existence of an axial electric field E_z and of an azimuthal magnetic field $H_\theta = H$. Moreover, the existence of a z-traveling wave guided by the wire surface requires a radial electric field E_r hence, we have:

$$\begin{cases} \mathbf{E}(\omega, r, z) = (E_r(\omega, r)\,\vec{e}_r + E_z(\omega, r)\,\vec{e}_z)\;\; e^{-\gamma z} \\ \mathbf{H}(\omega, r, z) = (H(\omega, r)\,\vec{e}_\theta)\;\; e^{-\gamma z} \end{cases} \tag{2}$$

While the **H**-field is linearly polarized in the transverse plane, the **E**-field is elliptically polarized in the longitudinal plane. Regarding the calculation of the electromagnetic field components inside and outside the wire, the application of Maxwell equations yields:

$$\nabla \times \mathbf{H} = j\omega\varepsilon\mathbf{E} \rightarrow E_r = \frac{\gamma H}{j\omega\varepsilon}; \quad E_z = \frac{1}{j\omega\varepsilon r}\frac{d}{dr}(rH) \tag{3}$$

$$\nabla \times \mathbf{E} = -j\omega\mu\mathbf{H} \rightarrow \gamma E_r + \frac{d}{dr}E_z = j\omega\mu H \tag{4}$$

where $\varepsilon = \varepsilon_w = \varepsilon_0 - j\sigma_w/\omega$ and $\mu = \mu_w$ for $r < a$, but $\varepsilon = \varepsilon_0$ and $\mu = \mu_0$ for $r > a$. Note that for good conductors, and up to optical frequencies, the wire's conductivity σ_w is several orders of magnitude larger than the term $\omega\varepsilon_0$.

Substituting (3) into (4) leads to a Bessel differential equation on the magnetic field H:

$$x^2\frac{d^2H}{dx^2} + x\frac{dH}{dx} + \left(x^2 - 1\right)H = 0, \quad \begin{cases} x = gr \\ g = \sqrt{\gamma^2 + \omega^2\varepsilon\mu} \end{cases} \tag{5}$$

where x is a complex dimensionless variable related to the radial coordinate through proportionality factors g (for both media) with the meaning of radial propagation constants,

$$\begin{cases} g_w = a_w + jb_w = \sqrt{\gamma^2 + \omega^2\varepsilon_w\mu_w} = \sqrt{\gamma^2 - j\omega\sigma_w\mu_w} \\ g_0 = a_0 + jb_0 = \sqrt{\gamma^2 + \omega^2\varepsilon_0\mu_0} \\ \quad = \sqrt{\alpha^2 - \beta^2 + \beta_0^2 + 2j\alpha\beta} \end{cases} \tag{6}$$

The unknown γ^2 is several orders of magnitude smaller than $\omega\sigma_w\mu_w$ and can be neglected in the computation of g_w. To the contrary, g_0 depends critically on γ^2 and its real and imaginary parts are such that $b_0 > 0$ and $a_0 b_0 = \alpha\beta > 0$, since $\mathrm{Im}(\gamma^2) = \mathrm{Im}(g_0^2)$.

The solution of the differential equation in (5) can be written as a sum of two independent first-order functions of the Bessel family:

$$H(r) = \begin{cases} A_1 J_1(x) + \cancel{A_3} N_1(x) & \text{for } r < a \\ A_2 H_1^{(1)}(x) + \cancel{A_4} H_1^{(2)}(x) & \text{for } r > a \end{cases} \tag{7}$$

where the A_k constants are found from the boundary conditions $H(0) = 0, H(\infty) = 0$. Considering the asymptotic behavior of the Neumann function N_1 for small r, and of the second-kind Hankel function $H_1^{(2)}$ for large r, we must have $A_3 = 0$ and $A_4 = 0$. On the other hand, the constants A_1 and A_2 are found by considering the relationship between $H(a)$ and I from Ampère's law,

$$2\pi a H(a) = I = \int_0^a \sigma_w E_z 2\pi r dr = -\int_a^\infty j\omega\varepsilon_0 E_z 2\pi r dr \tag{8}$$

and by enforcing, at the interface $r = a$, the continuity of the tangential H-field, i.e., $A_1 J_1(g_w a) = A_2 H_1^{(1)}(g_0 a)$.

Note, parenthetically, that the rightmost identity in (8) states that the conduction current in the wire returns, through free space, in the form of displacement currents.

In conclusion, the **H**-field can be evaluated from

$$H(r) = \frac{I}{2\pi a} \cdot \begin{cases} \dfrac{J_1(g_w r)}{J_1(g_w a)} & \text{for } r \le a \\ \dfrac{H_1^{(1)}(g_0 r)}{H_1^{(1)}(g_0 a)} & \text{for } r \ge a \end{cases} \tag{9}$$

The axial and radial components of the **E**-field are obtained from $H(r)$, using (3) and (9):

$$E_z(r) = \frac{I}{2\pi a} \cdot \begin{cases} \dfrac{g_w J_0(g_w r)}{\sigma_w J_1(g_w a)} & \text{for } r \le a \\ \dfrac{g_0 H_0^{(1)}(g_0 r)}{j\omega\varepsilon_0 H_1^{(1)}(g_0 a)} & \text{for } r \ge a \end{cases} \tag{10}$$

$$E_r(r) = \frac{I}{2\pi a} \cdot \begin{cases} \dfrac{\gamma J_1(g_w r)}{\sigma_w J_1(g_w a)} & \text{for } r < \\ \dfrac{\gamma H_1^{(1)}(g_0 r)}{j\omega\varepsilon_0 H_1^{(1)}(g_0 a)} & \text{for } r > a \end{cases} \tag{11}$$

From (10), enforcing the continuity of E_z at the interface $r = a$, we get the transcendental characteristic equation that allows the numerical determination of the axial propagation constant $\gamma(\omega)$ of the guided surface wave,

$$\frac{g_0 H_0^{(1)}(g_0 a)}{j\omega\varepsilon_0 H_1^{(1)}(g_0 a)} = \frac{g_w J_0(g_w a)}{\sigma_w J_1(g_w a)} \tag{12}$$

where the left hand-side depends on the unknown γ, via g_0 in (6).

Confirming the continuity of the normal component of the total current density at the interface $r = a$, one can also see from (11) that $j\omega\varepsilon_0 E_r(a^+) = \sigma_w E_r(a^-)$, showing that $E_r(a^-)$ is negligibly small. Note, however, that the normal component of the electric displacement vector is not continuous at $r = a$, the discontinuity exists and determines the density of charge distributed over the surface of the wire, $\rho = \varepsilon_0 E_r(a^+) = \gamma I/(2\pi a j\omega)$. Integrating ρ around the wire's cylindrical surface, of infinitesimal unit length, gives the pul charge Q on the wire,

$$Q = 2\pi a\rho = \frac{\gamma I}{j\omega} \tag{13}$$

III. ENERGY FLOW, SKIN EFFECT, WAVE IMPEDANCE

The flow of energy in the SWTL is fully described by the complex Poynting vector, with axial and radial components:

$$\mathbf{S} = \frac{1}{2}\mathbf{E} \times \mathbf{H}^* = (S_z \vec{e}_z - S_r \vec{e}_r) e^{-2\alpha z}, \quad \begin{cases} S_z = \frac{1}{2} E_r H^* \\ S_r = \frac{1}{2} E_z H^* \end{cases} \tag{14}$$

While component S_z is related to wave transmission in free space parallel to the wire, the radial component S_r is related to wire losses.

The complex power associated to the inward flux of S_r across the wire surface, of infinitesimal unit length, is computed from (14), (9) and (10), yielding:

$$P_w = \int_0^{2\pi} \frac{1}{2} E_z(a) H^*(a) a d\theta = \underbrace{\left(\frac{g_w}{2\pi a \sigma_w} \frac{J_0(g_w a)}{J_1(g_w a)} \right)}_{Z_w = R_w + jX_w} I_{rms}^2 \tag{15}$$

where $g_w = \sqrt{-j\omega\sigma_w \mu_w}$.

Ordinary skin-effect theory [23] shows that the term Z_w in parenthesis is nothing less than the well-known pul skin effect impedance of the wire. Hence, from (15) and (12) we write:

$$Z_w = \frac{g_w}{2\pi a \sigma_w} \frac{J_0(g_w a)}{J_1(g_w a)} = \frac{g_0}{2\pi a j\omega\varepsilon_0} \frac{H_0^{(1)}(g_0 a)}{H_1^{(1)}(g_0 a)} \tag{16}$$

Taking into account the result in (10) for $E_z(r)$ at $r = a$, it also turns clear that Z_w in (16) relates the pul longitudinal voltage drop along the surface of the wire with its own current, $E_z(a) = Z_w I$, for any z.

At this stage, a pause may be convenient to plainly clarify the meaning of the pul skin-effect impedance Z_w, obtained in (15)-(16), which is a key tool (input data) for determining the main parameters of the Sommerfeld wave (propagation constants and characteristic impedance). Is the pul skin-effect impedance defined by ordinary skin-effect theory the same that we found in the context of surface waves? The answer is yes and no. Please, see Appendix A.

The complex power related to the axial flux of S_z through a transverse cross section of the SWTL is computed from (14) and (3),

$$P_z = \int_a^\infty \frac{1}{2} E_r(r) H^*(r)\, 2\pi r dr = \frac{2\pi\gamma}{j\omega\varepsilon_0} \int_a^\infty H_{rms}^2(r)\, r dr \tag{17}$$

or, with the help of (9),

$$P_z = \underbrace{\left(\frac{\gamma}{2\pi a^2 j\omega\varepsilon_0} \int_a^\infty \left| \frac{H_1^{(1)}(g_0 r)}{H_1^{(1)}(g_0 a)} \right|^2 r dr \right)}_{Z_c = R_c + jX_c} I_{rms}^2 \tag{18}$$

where the term set in parenthesis denotes the characteristic impedance Z_c of the axial surface wave guided by the wire.

Math details on the integration procedure leading to Z_c are offered in Appendix B, the conclusion being:

$$Z_c = \frac{\gamma}{4\pi a j\omega\varepsilon_0} \mathrm{Im}\left(\frac{g_0}{a_0 b_0} \frac{H_0^{(1)}(g_0 a)}{H_1^{(1)}(g_0 a)} \right) \tag{19}$$

or, more compactly, using the rightmost identity in (16),

$$Z_c = R_c + jX_c = \frac{\gamma R_w}{2j\alpha\beta} = \frac{R_w}{2\alpha} - j\frac{R_w}{2\beta} \tag{20}$$

The result in (20), where the identity $a_0 b_0 = \alpha\beta$ was used, shows that the characteristic wave impedance Z_c is a complex of the 4th quadrant, orthogonal to γ, that is:

$$\alpha R_c + \beta X_c = 0 \tag{21}$$

IV. PROPAGATION PARAMETERS ESTIMATION FOR LOW FREQUENCIES

The transcendental equation in (12) for the computation of the axial propagation constant γ can be rewritten explicitly and conveniently in terms of the pul skin effect impedance of the wire Z_w. From (12) and (16), we find:

$$\begin{cases} x \dfrac{H_0^{(1)}(x)}{H_1^{(1)}(x)} = 2\pi a^2 j\omega\varepsilon_0 |Z_w| e^{j\theta_w} \\ x = g_0 a = |g_0 a| e^{j\theta_0}, \quad \gamma = \sqrt{(x/a)^2 - \beta_0^2} \end{cases} \tag{22}$$

where θ_w and θ_0 are, respectively, the angles of Z_w and g_0, both of the first quadrant.

Now we consider that the frequency is low enough to ensure that $|x| \ll 1$, in which case the ratio of the Hankel functions is given by the following approximation [7],

$$\frac{H_0^{(1)}(x)}{H_1^{(1)}(x)} \approx x \ln \frac{j\varsigma}{x} = x \ln \left|x^{-1}\right| \left(1 + \frac{\ln\varsigma + j\left(\frac{\pi}{2} - \theta_0\right)}{\ln \left|x^{-1}\right|} \right) \approx x \ln \left|x^{-1}\right| \tag{23}$$

where $\varsigma = 2/e^m \approx 1.123$, and m is the Euler-Mascheroni constant ($m = 0.57721\cdots$). Note that the last simplification in (23) will be acceptable provided that $\left|x^{-1}\right|$ is very large, which is true for very small x.

Hence, from (22)-(23), we find:

$$\left|g_0^2\right| \ln \left| \frac{1}{g_0 a} \right| e^{j2\theta_0} \approx 2\pi j\omega\varepsilon_0 Z_w = 2\pi\omega\varepsilon_0 |Z_w| e^{j(\theta_w + \frac{\pi}{2})} \tag{24}$$

Owing to the presence of the logarithm function in (24) the latter equation cannot yield a closed form accurate solution for g_0; however, the angle θ_0 of the radial propagation constant can be easily estimated.

In fact, from (24), we see that the complex quantities Z_w and g_0^2 are approximately orthogonal, making an angle near to $\pi/2$, hence we may write:

$$\begin{cases} \mathrm{Re}(g_0^2) R_w \approx \mathrm{Im}(g_0^2) X_w \\ (\alpha^2 - \beta^2 + \beta_0^2) R_w \approx 2\alpha\beta X_w \\ \theta_0 \approx \dfrac{1}{2}\left(\theta_w + \dfrac{\pi}{2}\right) \end{cases} \tag{25}$$

from where we obtain

$$\begin{cases} \text{If } X_w \ll R_w \text{ then } \theta_0 \approx \dfrac{\pi}{4} \text{ and } \beta^2 - \beta_0^2 \approx \alpha^2 \\ \text{If } X_w \approx R_w \text{ then } \theta_0 \approx \dfrac{3\pi}{8} \text{ and } \beta^2 - \beta_0^2 \approx 2\alpha\beta \end{cases} \tag{26}$$

V. PUL TRANSMISSION LINE PARAMETERS

The wave parameters γ and Z_c determined in the preceding sections fully describe surface wave propagation along the SWTL. Despite that, mimicking the established practice in ordinary quasi-TEM transmission-line analysis, various authors [12], [14], [20], [21], [22], [25], [26] have referred the utilization of pul inductance and capacitance parameters to characterize the wave behavior of SWTL.

We have been sceptic about the utilization of these pul parameters in SWTL analysis, where **E**-field lines start and end at the single wire itself (Fig. 1) since no other conductor exists —see discussion in [25] and [26]. Nonetheless, we decided to reexamine the subject, proceeding to the determination of those pul parameters employing various approaches with different physical supports —which, not surprisingly, produce different results, but surprisingly, not very different, in fact identical to first-order approximation.

A. TEM APPROACH

Based on the knowledge of the propagation constant γ and characteristic impedance Z_c of the axial wave, the TEM approach mimics the procedure used in ordinary TL analysis: The pul transverse admittance and pul longitudinal impedance are firstly obtained and then, from them, the pul parameters C_0 and L_0 are calculated.

In the framework of ordinary two-wire line quasi-TEM theory, the wave parameters γ and Z_c are related to the pul longitudinal impedance Z_l and pul transverse admittance Y_t through [23]:

$$\begin{cases} Z_c = \sqrt{Z_l Y_t^{-1}} \\ \gamma = \sqrt{Z_l Y_t} \end{cases}, \quad \begin{cases} Y_t = \gamma Z_c^{-1} = G + j\omega C_0 \\ Z_l = \gamma Z_c = R + j\omega L = Z_w + j\omega L_0 \end{cases} \tag{27}$$

where L_0 and C_0 are the pul external inductance and capacitance of the line, G is the pul transverse conductance associated with dielectric losses, and Z_w is the wires' pul internal impedance associated to skin effect phenomena (whose real part R_w accounts for energy dissipation). Moreover, if the dielectric medium around the wires is free space without dielectric losses, as assumed in this work, then one will have $Y_t = j\omega C_0$ and $C_0 L_0 = \varepsilon_0 \mu_0 = 1/c^2$.

Adopting the two-wire transmission line formalism in (27) to the SWTL problem, using (20), yields:

$$Y_t = \frac{\gamma}{Z_c} = \frac{2j\alpha\beta}{R_w} \rightarrow C_0(\omega) = \frac{Y_t}{j\omega} = \frac{2\alpha\beta}{\omega R_w} \tag{28}$$

and

$$\begin{cases} Z_l = \gamma Z_c = \dfrac{\gamma^2 R_w}{2j\alpha\beta} = R_w + jR_w\left(\dfrac{\beta^2 - \alpha^2}{2\alpha\beta}\right) \\ L_0(\omega) = \dfrac{Z_l - Z_w}{j\omega} = \dfrac{\beta_0^2 R_w}{2\alpha\beta\omega}\left(\dfrac{\beta^2 - 2\alpha\beta X_w/R_w - \alpha^2}{\beta_0^2}\right) \end{cases} \tag{29}$$

The pul capacitance C_0 and pul inductance L_0 are real valued functions of the frequency.

The problem with this approach is revealed by two aspects. The inductance L_0 may turn into a negative quantity (a non-physical situation) when $\alpha > \beta$, which may happen at very low frequencies. In addition, the product

$$C_0 L_0 = \frac{1}{c^2}\left(\frac{\beta^2 - 2\alpha\beta X_w/R_w - \alpha^2}{\beta_0^2}\right) \tag{30}$$

not only does not coincide with $1/c^2$ but, also, may become negative.

B. CIRCUIT APPROACH

The circuit approach employs the quasi-static definitions of capacitance and inductance based on the familiar ratios charge /voltage and flux /current. The pul charge on the wire's surface is divided by the radial voltage to yield C_0. The pul magnetic flux around the wire is divided by the wire current to yield L_0.

With regard to the pul capacitance we have [12],

$$C_0 = \frac{Q(z)}{V(z)} = \frac{\gamma I/(j\omega)}{\int_a^\infty E_r(z, r)dr} \tag{31}$$

where Q is the pul charge on the wire's surface defined in (13), and the voltage V in the denominator, defined as the radial integration of the **E**-field in a transverse plane from a point at the wire's surface ($r = a$) to a point at infinity, [12], [19], [20], can be evaluated using (11) and (16), yielding:

$$V = \frac{\gamma I}{2\pi j\omega\varepsilon_0} \cdot \frac{H_0^{(1)}(g_0 a)}{g_0 a\, H_1^{(1)}(g_0 a)} = \frac{\gamma Z_w}{g_0^2} I \tag{32}$$

Plugging (32) into (31) gives:

$$C_0(\omega) = \frac{g_0^2}{j\omega Z_w} = \frac{2\alpha\beta}{\omega R_w}\left(\frac{1 + j(\beta^2 - \beta_0^2 - \alpha^2)/(2\alpha\beta)}{1 + jX_w/R_w}\right) \tag{33}$$

With regard to the pul inductance L_0 we have, [12],

$$L_0 = \frac{\psi(z)}{I(z)} = \int_a^\infty \mu_0 H(z, r)dr/I(z) \tag{34}$$

where ψ denotes the magnetic flux across a rectangular surface on the rz-plane, of infinite radial extent $r \in [a, \infty[$, and

infinitesimal unit length. Using (9) for $H(r)$ leads to:

$$L_0(\omega) = \frac{\mu_0}{2\pi}\frac{H_0^{(1)}(g_0 a)}{g_0 a\, H_1^{(1)}(g_0 a)} = \mu_0\varepsilon_0\frac{j\omega Z_w}{g_0^2} = \frac{\beta_0^2 R_w}{2\alpha\beta\omega}\left(\frac{1+jX_w/R_w}{1+j(\beta^2-\beta_0^2-\alpha^2)/(2\alpha\beta)}\right) \quad (35)$$

In this approach none of the pul parameters is a real valued function, both the inductance and capacitance are complex. Curiously, their product coincides with $1/c^2$.

Another difficulty with the circuit approach is that the radial voltage V involved in the definition of capacitance, (31), is an unmeasurable voltage, therefore unphysical.

C. ENERGY APPROACH

As the name suggests, the energy approach is based on the calculation of the energy stored in the electromagnetic field around the wire. The square of the pul wire's charge is divided by the pul electric energy to yield C_0. The pul magnetic energy is divided by the square of the wire's current to yield L_0.

The energy-based approach for the calculation of the pul parameters of the SWTL has a clear advantage over the other two already examined. This approach leads to parameters L_0 and C_0 that, by definition, are intrinsically real and positive, for energies are quadratic forms.

For the calculation of C_0 we employ the well-known relation between stored electric energy and electric charge

$$(W_e)_{av} = \int_V \left(\hat{w}_e\right)_{av} dV = \frac{1}{2}\frac{Q_{rms}^2}{C_0} \rightarrow C_0 = \frac{1}{4}\frac{QQ^*}{(W_e)_{av}} \quad (36)$$

where $\left(\hat{w}_e\right)_{av} = \frac{1}{2}\varepsilon_0 E_{rms}^2$ is the time-averaged density of the electric energy, and the volume of integration is a circular disk of infinite radial extent, $r \in [a,\ \infty[$, with unit length infinitesimal thickness.

Since the **E**-field is elliptically polarized in the rz-plane, its root-mean-square value obeys $E_{rms}^2 = (E_r^2)_{rms} + (E_z^2)_{rms}$, and, therefore,

$$(W_e)_{av} = W_r + W_z, \begin{cases} W_r = \pi\varepsilon_0 \int_a^\infty (E_r^2)_{rms} r dr \\ W_z = \pi\varepsilon_0 \int_a^\infty (E_z^2)_{rms} r dr \end{cases} \quad (37)$$

From (3), we see that fields E_r and H are proportional, consequently, the integral W_r turns into an integral on $|H|^2$, which was solved earlier in Appendix B when calculating the characteristic impedance Z_c of the SWTL. Then, using (17)-(20), we readily obtain

$$W_r = \pi\varepsilon_0\left|\frac{\gamma}{\omega\varepsilon_0}\right|^2 \int_a^\infty H_{rms}^2 r dr = \mathrm{Re}\left(\frac{\gamma\gamma^*}{2\alpha\beta}Z_w^*\right)\frac{I_{rms}^2}{2\omega} = \left(\frac{\beta^2+\alpha^2}{2\alpha\beta}\right)\frac{R_w I_{rms}^2}{2\omega} \quad (38)$$

Field components E_z and H are not proportional. Details on the calculation of W_z are offered in Appendix C, the output result being:

$$W_z = \pi\varepsilon_0 \int_a^\infty (E_z^2)_{rms} r dr = \mathrm{Re}\left(\frac{g_0^2}{2\alpha\beta}Z_w^*\right)\frac{I_{rms}^2}{2\omega} = \left(\frac{X_w}{R_w} + \frac{\beta_0^2-\beta^2+\alpha^2}{2\alpha\beta}\right)\frac{R_w I_{rms}^2}{2\omega} \quad (39)$$

From (36)-(39), making $QQ^* = 2|\gamma I_{rms}/\omega|^2$ in (36), yields the pul capacitance:

$$C_0(\omega) = \frac{2\alpha\beta}{\omega R_w}\left(\frac{\beta^2+\alpha^2}{\beta_0^2 + 2\alpha\beta X_w/R_w + 2\alpha^2}\right) \quad (40)$$

The calculation of the pul inductance L_0 via the stored magnetic energy is straightforward because the **H**-field is linearly polarized in the transverse plane. Now, we have:

$$L_0 = \frac{2\,(W_m)_{av}}{I_{rms}^2} = \frac{2}{I_{rms}^2}\int_V \frac{1}{2}\mu_0 H_{rms}^2 dV = \frac{2\pi\mu_0}{I_{rms}^2}\int_a^\infty H_{rms}^2 r dr \quad (41)$$

and, from (17)-(20):

$$L_0(\omega) = \mu_0\varepsilon_0\frac{\omega R_w}{2\alpha\beta} = \frac{\beta_0^2 R_w}{2\alpha\beta\omega} \quad (42)$$

The pul capacitance and pul inductance are positive real valued functions of the frequency but, again, their product:

$$C_0 L_0 = \frac{1}{c^2}\left(\frac{\beta^2+\alpha^2}{\beta_0^2 + 2\alpha\beta X_w/R_w + 2\alpha^2}\right) \quad (43)$$

does not coincide with $1/c^2$.

VI. COMPUTATION RESULTS AND DISCUSSION

To provide the reader with numerical data on the typical values of the radial and axial wave parameters of the SWTL, we start this Section focusing on the complex quantities $Z_w(\omega)$, $g_0(\omega)$, $\gamma(\omega)$ and $Z_c(\omega)$, whose angles, real and imaginary parts were computed numerically using the exact equations in Sections II and III.

Results are listed in Tables 1–4, for a few frequencies between 1 Hz and 1 GHz, for a copper wire ($\mu = \mu_0$, $\sigma_w = 56$ MS/m) of 1 mm radius.

Table 1 shows that the transition from weak to strong skin effect takes place above 1 kHz (precisely at 4.5 kHz) when the skin depth and the wire radius turn equal.

Table 2 concerns the real and imaginary parts of the radial propagation constant $g_0(\omega)$, whose magnitude and angle are plotted against frequency in Fig. 2. The log-log plot of $|g_0|$ reveals that this function has two asymptotes with approximate slopes of 1/2 and 3/4; this suggests that the modulus $|g_0|$ increases with $\sqrt{\omega}$ for weak skin effect, but with $\sqrt{\omega^{3/2}}$ for strong skin effect —this conclusion supports the approximation in (24). In Fig. 2 we added a dashed line showing

TABLE 1. Pul skin effect impedance, $Z_w = R_w + jX_w$ (Ω/m).

Frequency	R_w	X_w	θ_w
1 Hz	$5.6841\ 10^{-3}$	$3.1416\ 10^{-7}$	0.0032°
1 kHz	$5.6899\ 10^{-3}$	$3.1400\ 10^{-4}$	3.1587°
1 MHz	$4.3714\ 10^{-2}$	$4.2219\ 10^{-2}$	44.003°
1 GHz	$1.3377\ 10^{0}$	$1.3363\ 10^{0}$	44.970°

TABLE 2. Radial propagation constant, $g_0 = a_0 + jb_0$ (m^{-1}).

Frequency	a_0	b_0	θ_0
1 Hz	$2.1605\ 10^{-7}$	$2.0833\ 10^{-7}$	43.958°
1 kHz	$7.2860\ 10^{-6}$	$7.3817\ 10^{-6}$	45.374°
1 MHz	$5.0352\ 10^{-4}$	$1.1379\ 10^{-3}$	66.132°
1 GHz	$1.1460\ 10^{-1}$	$2.5788\ 10^{-1}$	66.041°

TABLE 3. Axial propagation constant, $\gamma = \alpha + j\beta$ (m^{-1})

Frequency	α	β	θ_γ
1 Hz	$2.1552\ 10^{-7}$	$2.0884\ 10^{-7}$	44.098°
1 kHz	$2.5435\ 10^{-6}$	$2.1145\ 10^{-5}$	83.141°
1 MHz	$2.7306\ 10^{-5}$	$2.0983\ 10^{-2}$	89.925°
1 GHz	$1.4100\ 10^{-3}$	$2.0960\ 10^{1}$	89.996°

TABLE 4. Characteristic impedance, $Z_c = R_c + jX_c$ (Ω)

Frequency	R_c	$-X_c$	$-\theta_c$
1 Hz	$1.3187\ 10^{4}$	$1.3609\ 10^{4}$	45.902°
1 kHz	$1.1185\ 10^{3}$	$1.3454\ 10^{2}$	6.8589°
1 MHz	$8.0045\ 10^{2}$	$1.0416\ 10^{0}$	0.0746°
1 GHz	$4.7437\ 10^{2}$	$3.1912\ 10^{-2}$	0.0039°

the approximate representation of $\theta_0(\omega)$ based on the quasi orthogonality of Z_w and g_0^2, (25).

Table 3 shows that at 1 Hz (extremely low frequency) the axial attenuation constant α exceeds the phase constant β, contrarily, above 1 MHz, the phase constant is already three orders of magnitude larger than α. Table 4 depicts a similar trend in the characteristic wave impedance; the reactance X_c exceeds the resistance R_c for extremely low frequencies, but above 1 MHz the resistance is already three orders of magnitude larger than X_c, confirming (21).

Next, we computed and examined the per unit length C_0 and L_0 parameters of the SWTL investigated in Section V. Two materials were considered: copper, again, as an example of a nonmagnetic very good conductor, and carbon steel as an example of a magnetic good conductor.

A. NONMAGNETIC WIRE

The pul parameters C_0 and L_0 were numerically evaluated against frequency for the case of a copper wire, considering two values of the wire radius, $a = 1$ mm and $a = 1$ cm.

The subplots in Fig. 3 depict the normalized functions $C_0(\omega)/\varepsilon_0$ and $L_0(\omega)/\mu_0$ for $a = 1$ mm, calculated using

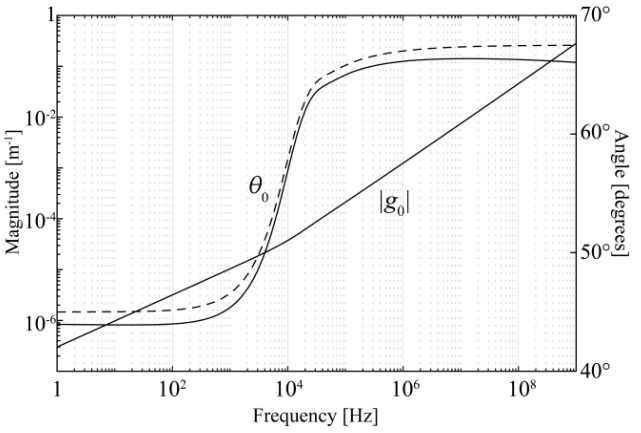

FIGURE 2. Magnitude and angle plots of the radial propagation constant $g_0(\omega)$ against frequency. The dashed line shows the angle approximation given by (25).

the various approaches presented in Section V. The same in Fig. 4, but for $a = 1$ cm.

Note, in both figures, that the imaginary parts of C_0 and L_0 (circuit approach) are also displayed, represented by dashed lines, using a 10-times expanded scale (scale on the right-hand side).

Observation of the numerical results in Fig. 3 and Fig. 4 shows:

- The curves T (black), C (red) and E (blue) do not coincide in the whole frequency range but largely overlap in some regions; curves T and C tend to overlap at frequencies where the skin effect is weak; conversely, when the skin effect is strong, the overlap occurs with curves T and E.

- For all the approaches, the pul capacitance increases with increasing ω, from about $\varepsilon_0/4$ to ε_0; the inverse happens to the pul inductance that decreases from about $4\mu_0$ to μ_0.

- An exception to the above remark is the curve T for the pul inductance that exhibits non-physical negative values at extremely low frequencies; but in the remaining frequency range the curve T turns positive and merges with the curves C and E.

- It is also confirmed that the circuit approach leads to non-physical imaginary parts in the pul parameters L_0 and C_0 (dashed lines), but their amplitude is small, some 2 orders of magnitude smaller than the corresponding real parts.

- The curves of C_0 and L_0 for $a = 1$ mm and $a = 1$ cm are similar; the curves in Fig. 3 and Fig. 4 show the same trend, diverging slowly as f increases to 1 GHz. Nonetheless, for the circuit approach, noticeable differences can be observed in the plots of the imaginary parts of L_0 and C_0, not in their amplitudes (which are kept small) but on the specific frequencies where sudden variations occur —the frequency location diminishes 2 orders of magnitude, from 10^4 Hz to 10^2 Hz when the wire radius increases one order of magnitude. Those frequencies are the transition frequencies from weak to strong skin effect defined by the condition $a \approx \delta$ (with δ the skin depth, proportional to $\omega^{-1/2}$).

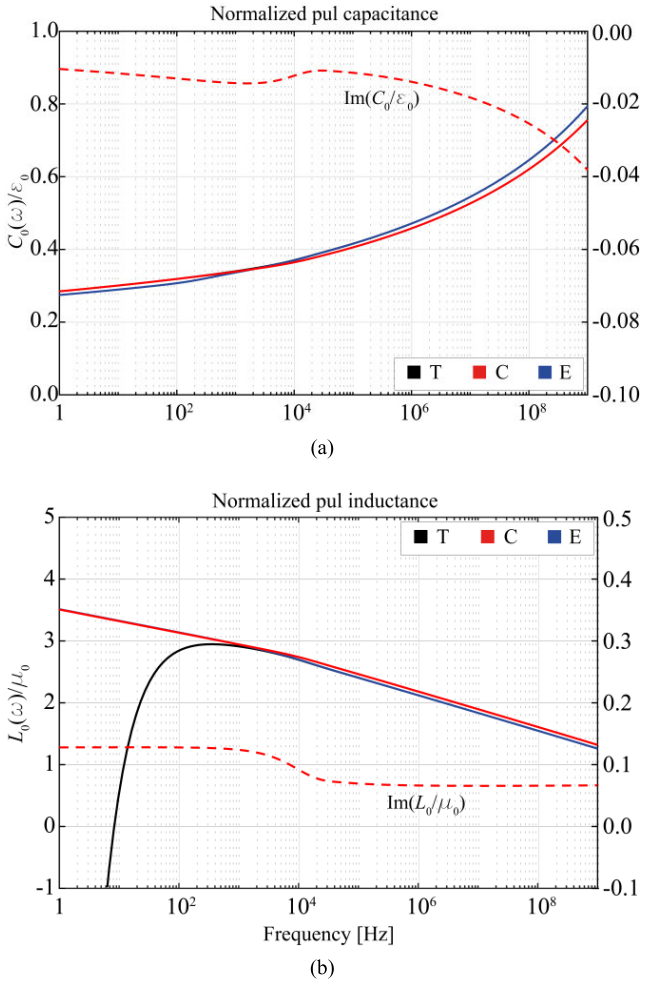

FIGURE 3. Pul parameters of the SWTL against frequency for a copper wire of radius a = 1 mm, calculated using the TEM-approach (T), the circuit approach (C), and the energy approach (E). Subplot (a) shows the normalized capacitance $C_0(\omega)/\varepsilon_0$, subplot (b) shows the normalized inductance $L_0(\omega)/\mu_0$. The dashed lines in (a) and (b) show, respectively, the non-zero imaginary parts of the pul normalized capacitance and inductance found using the circuit approach (scale on the right).

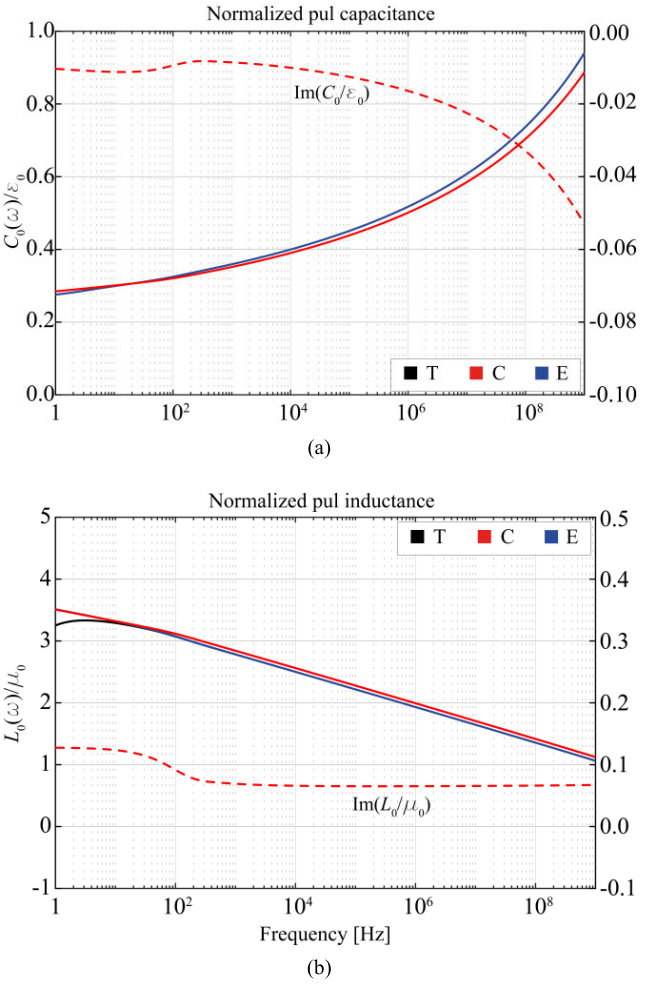

FIGURE 4. Pul parameters of the SWTL against frequency for a copper wire of radius a = 1 cm, calculated using the TEM-approach (T), the circuit approach (C), and the energy approach (E). Subplot (a) shows the normalized capacitance $C_0(\omega)/\varepsilon_0$, subplot (b) shows the normalized inductance $L_0(\omega)/\mu_0$. The dashed lines in (a) and (b) show, respectively, the non-zero imaginary parts of the pul normalized capacitance and inductance found using the circuit approach (scale on the right).

The analytical results established in Section V for the TEM approach (28), (29), for the circuit approach (33), (35), and for the energy approach (40), (42), fail to coincide; this means that the object of calculation lacks a deep physical meaning. Nevertheless, all the approaches produce similar results, with a common dominant term.

For the approach K (with K = T, C, E) the various pul capacitances and pul inductances can be rewritten in the compact form:

$$C_0^K = C_0(1+\chi_C^K), \quad L_0^K = L_0(1+\chi_L^K), \text{ for } K = T, C, E \tag{44}$$

where the common dominant terms are:

$$C_0 = \frac{2\alpha\beta}{\omega R_w}, \quad L_0 = \frac{\beta_0^2 R_w}{2\alpha\beta\omega} = \frac{\mu_0\varepsilon_0}{C_0} \tag{45}$$

Note, from (45), that the normalized quantities C_0/ε_0 and L_0/μ_0 are the inverse of each other, as the simulations already suggested.

The quantities χ_C^K and χ_L^K in (44) can be interpreted as first order corrections to the common dominant term. Those corrections are not only frequency-dependent but also approach-dependent. They can be extracted from (28), (29), (33), (35), (40), (42), and are summarized below:

$$\text{TEM-approach} \begin{cases} \chi_C^T = 0 \\ \chi_L^T = \dfrac{N}{\beta_0^2} \end{cases} \tag{46}$$

$$\text{Circuit-approach} \begin{cases} \chi_C^C = \dfrac{N}{2\alpha\beta(X_w/R_w - j)} \\ \chi_L^C = \dfrac{N}{j2\alpha\beta - (\beta^2 - \beta_0^2 - \alpha^2)} \end{cases} \tag{47}$$

$$\text{Energy-approach} \begin{cases} \chi_C^E = \dfrac{N}{\beta_0^2 + 2\alpha^2 + 2\alpha\beta X_w/R_w} \\ \chi_L^E = 0 \end{cases} \tag{48}$$

where:

$$N = (\beta^2 - \beta_0^2 - \alpha^2) - 2\alpha\beta X_w/R_w \tag{49}$$

Observe that the numerators N in (46)-(48) are all the same and given by the expression in (49). Going back to Section V we may recall that the complex quantities Z_w and g_0^2 are approximately orthogonal, and, from (24)-(25), we find that $N \approx 0$. With no exception, all the χ terms remarkably collapse to zero,

$$\chi_C^K \approx \chi_L^K \approx 0, \quad \text{for } K = T, C, E \tag{50}$$

As to the various approaches compared in Figs. 3 and 4, the differences among the graph plots of the pul parameters (capacitances and inductances) are so small because they are of second order importance, indeed. Hence, albeit our initial skepticism about the usage of pul parameters, it seems that the results in (45), common to the three approaches, can be adopted as a sound first order approximation at least for low frequencies (below 1 GHz).

The equation in (24), key for recognizing that N in (46)-(49) is zero at first order approximation, can also be used to help explain why $C_0 \approx \varepsilon_0/k$ and $L_0 \approx \mu_0 k$, where k is a frequency-dependent real positive quantity varying approximately in the range 1 to 4. In fact, extracting the imaginary part of both sides of (24) leads to:

$$\begin{cases} \text{Im}(g_0^2) = 2a_0 b_0 \approx \dfrac{2\pi\varepsilon_0}{\ln|1/(g_0 a)|}\omega \text{Im}(jZ_w) \\ 2\alpha\beta \approx \dfrac{2\pi\varepsilon_0}{\ln|1/(g_0 a)|}\omega R_w \end{cases} \tag{51}$$

and, from (45),

$$C_0 \approx \frac{2\pi\varepsilon_0}{\ln\left|g_0^{-1}/a\right|}, \quad L_0 \approx \frac{\mu_0}{2\pi}\ln\left|g_0^{-1}/a\right| \tag{52}$$

Therefore, we find that $k = \frac{1}{2\pi}\ln|1/(g_0 a)|$. For $a = 1$ mm, and since $|g_0(\omega)|$ increases from 10^{-7} to 10^{-1} (see Fig. 2), the value of k will decrease from 4 to 1, as illustrated in the graphs of C_0 and L_0 in Fig. 3.

The results in (52) seem to suggest that from the viewpoint of the pul constitutive parameters, C_0 and L_0, the SWTL is equivalent to a coaxial cable with inner radius a (= 1 mm) and outer radius equal to $|g_0^{-1}(\omega)|$, some 2 m at 1 GHz, but more than 3000 km at 1 Hz.

B. MAGNETIC WIRE

To the best of our knowledge, research on surface wave propagation has not so far considered the case of conducting wires with magnetic properties (magnetic wires). However, as mentioned in Section I, electromagnetic models based on the Sommerfeld wave are being implemented to characterize the behavior of power line steel towers struck by lightning currents [18], [19] —return conductor absent in the path of the return current.

Steel is a conducting magnetic medium whose magnetic properties will be here approximated by a basic Debye's model [28], [29], through:

$$\mu_w(\omega) = |\mu_w|\, e^{-j\theta_\mu} = \mu_r - j\mu_i = \mu_\infty + \frac{\mu_{dc} - \mu_\infty}{1 + j\omega/\omega_0} \tag{53}$$

where μ_{dc} and μ_∞ are permeability values for $\omega = 0$ and $\omega \to \infty$, and ω_0 is the ferromagnetic resonance frequency —see Fig. 5. Also, according to Snoek's limit [30], we take $\mu_\infty \approx \mu_0$ in (53).

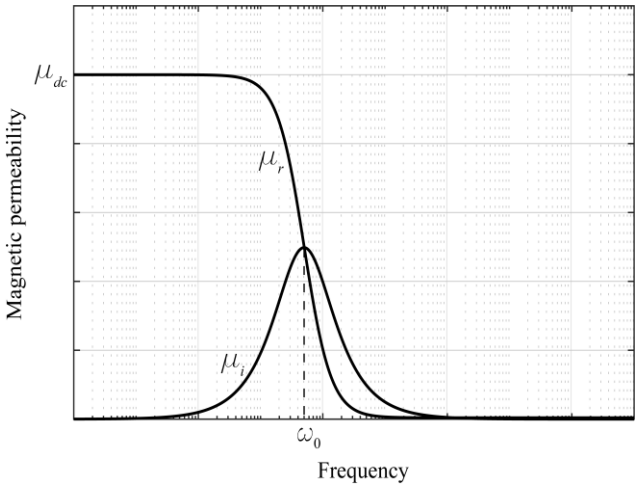

FIGURE 5. Real and imaginary parts of the magnetic wire's frequency-dependent complex permeability (Debye model).

Since the case of magnetic SWTL has not been addressed in the literature, we pay here special attention to it by thoroughly illustrating the effects of the frequency-dependent complex permeability on the computation of the skin effect impedance, wave parameters (axial and radial propagation), and pul parameters (considering the T, C and E approaches).

As data, we take a carbon steel wire with $a = 1$ cm, $\sigma_w = 5$ MS/m, $\mu_{dc} = 250\mu_0$ and $f_0 = 5$ kHz, [29].

Fig. 6 shows the real and imaginary parts of the wire pul skin effect impedance against frequency, for $f < 0.1$ MHz (Fig. 6a) and $f > 0.1$ MHz (Fig. 6b). Also, from Fig. 7 (radial propagation constant), useful information about the skin effect angle θ_w can be extracted from the dashed line —recall, from (25), that $\theta_w \approx 2\theta_0 - \pi/2$. The curves in Fig. 6 have no similarity whatsoever with the familiar curves of R_w and X_w for nonmagnetic wires (check with Fig. 10 in Appendix A). This requires an explanation.

For extremely low frequencies (weak skin effect, [23]) we write:

$$Z_w \approx \underbrace{\left(\frac{1}{\pi a^2 \sigma_w}\right)}_{R_{dc}} + j\frac{\omega\mu_w}{8\pi} \to \begin{cases} R_w \approx R_{dc} + \dfrac{\omega\mu_{dc}}{8\pi}\dfrac{\omega}{\omega_0} \\ X_w \approx \dfrac{\omega\mu_{dc}}{8\pi} \end{cases} \tag{54}$$

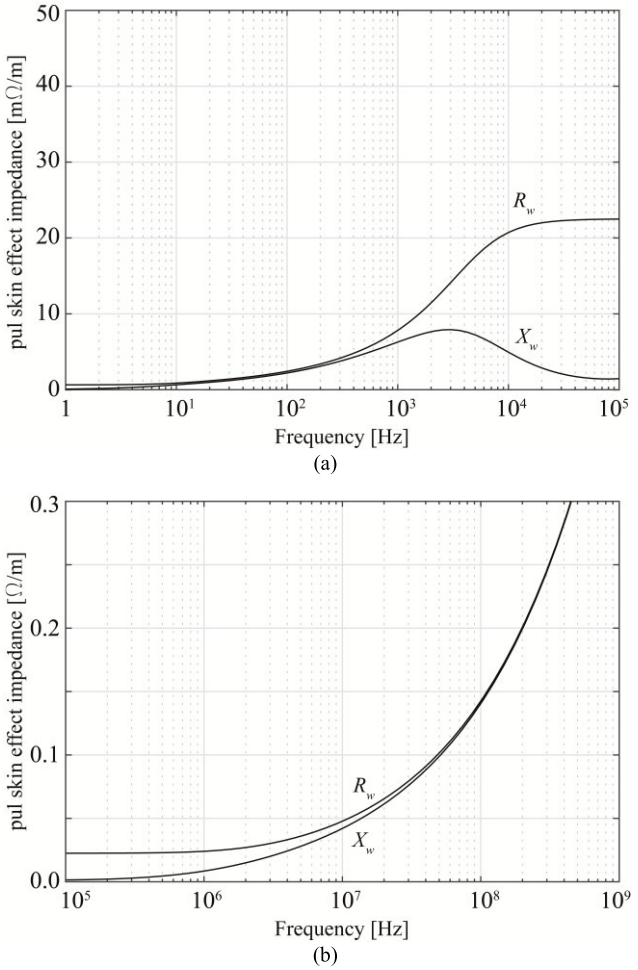

FIGURE 6. Real and imaginary parts of the pul skin effect impedance of the magnetic SWTL against frequency. (a) f < 0.1 MHz; (b) f > 0.1 MHz.

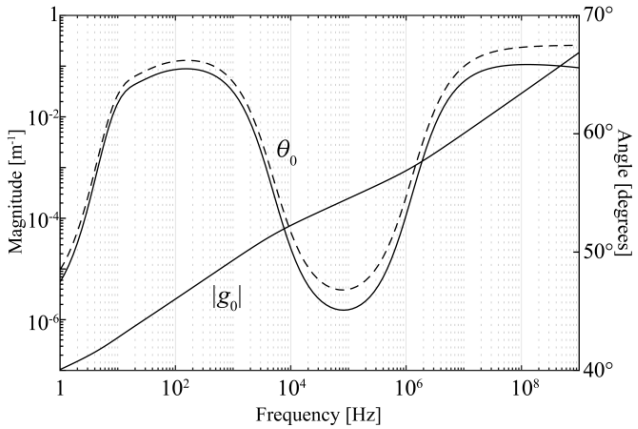

FIGURE 7. Magnitude and angle of the radial propagation constant $g_0(\omega)$ of the magnetic SWTL against frequency. The log-log plot of $|g_0|$ shows three regions, from 1 Hz to 5 kHz with slope 3/4, from 5 kHz to 1 MHz with slope 1/2, and above 1 MHz again with slope 3/4. The dashed line shows the angle approximation given by (25), $\theta_0 = 45° + \theta_w/2$.

For direct current, we have $\theta_w = 0$, but just a small increase in the frequency —less than 10 Hz— makes the angle θ_w rapidly grow to near 45°.

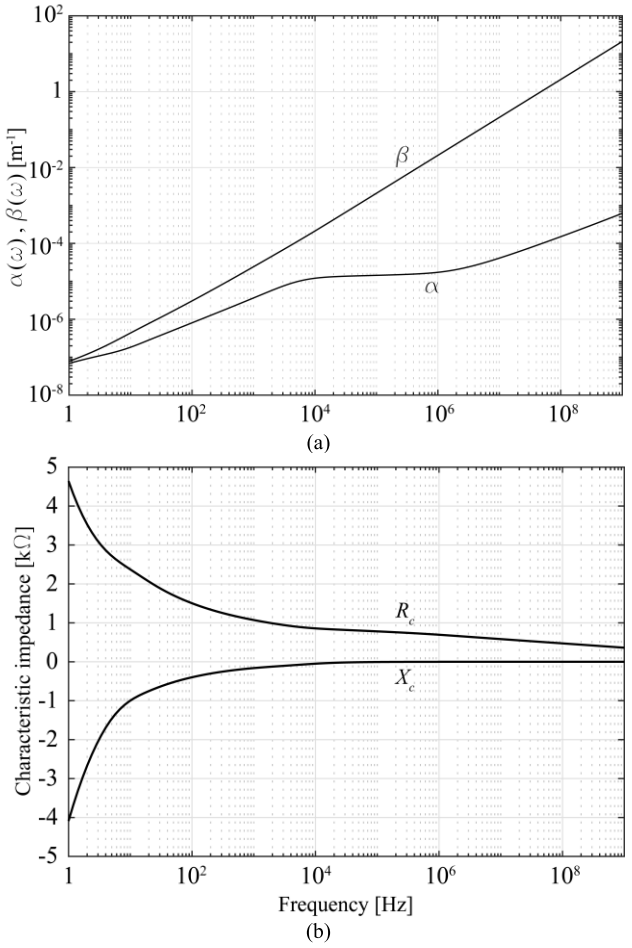

FIGURE 8. Axial wave parameters of the magnetic SWTL against frequency. (a) Attenuation and phase constants. (b) Characteristic wave resistance and reactance.

At intermediate frequencies, from 10 Hz to 1 kHz, where (54) does not apply, the angle θ_w remains near to 45°, with $R_w \approx X_w$. Afterwards, θ_w drops to near zero again (as if in dc). To understand this behavior, we must consider the strong skin effect approximation [23], and write:

$$\begin{cases} Z_w \approx \dfrac{1+j}{2\pi a \delta \sigma_w} = R_\delta \sqrt{2} e^{j(\pi/2-\theta_\mu)/2} \\ R_\delta = \dfrac{1}{2\pi a\,|\delta|\,\sigma_w}, \quad \delta = \sqrt{\dfrac{2}{\omega\,|\mu_w|\,\sigma_w}}\, e^{j\theta_\mu/2} \end{cases} \tag{55}$$

where R_δ is the pul skin resistance and δ is the wire's skin depth (an ever-decreasing function of the frequency) which, is characterized not only by its absolute value but also by its angle (half of the permeability angle). Then, from (55), after some trigonometry, we find:

$$\begin{cases} Z_w \approx \underbrace{R_\delta \sqrt{1+\sin\theta_\mu}}_{R_w} + j \underbrace{R_\delta \sqrt{1-\sin\theta_\mu}}_{X_w} \\ \theta_w \approx \arctan \sqrt{\dfrac{1-\sin\theta_\mu}{1+\sin\theta_\mu}} \end{cases} \tag{56}$$

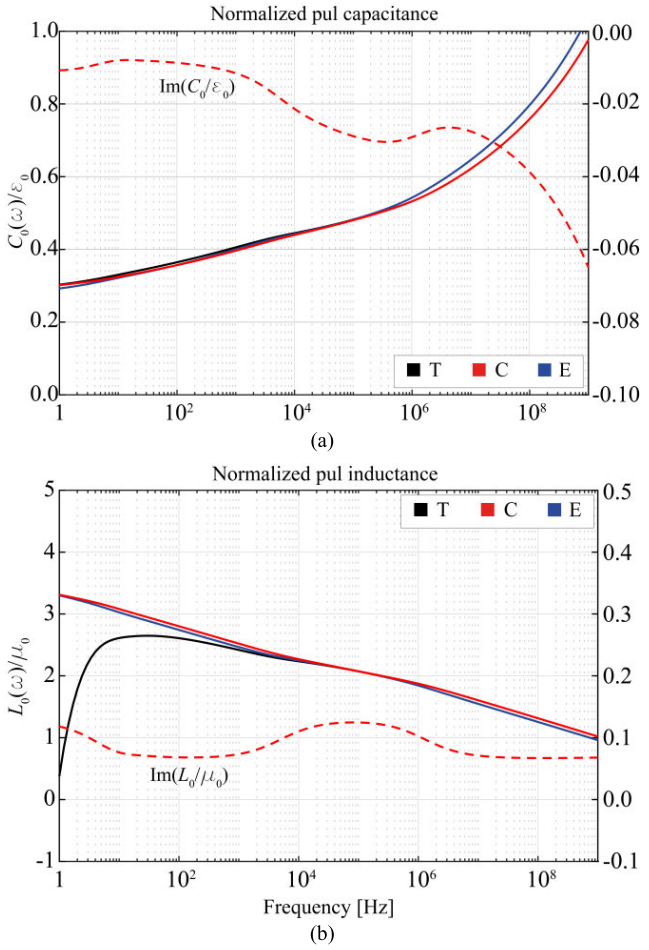

FIGURE 9. Pul parameters of the magnetic SWTL against frequency, calculated using the TEM approach (T), the circuit approach (C), and the energy approach (E). Subplot (a) shows the normalized capacitance $C_0(\omega)/\varepsilon_0$, subplot (b) shows the normalized inductance $L_0(\omega)/\mu_0$. The dashed lines in (a) and (b) show, respectively, the non-zero imaginary parts of the pul normalized capacitance and inductance for the circuit approach (scale on the right).

Since θ_w falls to near zero (at around 80 kHz) then the permeability angle must get near to 90°. Observing Fig. 5 we see that this is possible for $\omega > \omega_0$, when μ_i exceeds μ_r.

The modulus and angle of the permeability can be easily calculated from (53), yielding:

$$|\mu_w| = \sqrt{\frac{\mu_{dc}^2 + (\mu_0 \frac{\omega}{\omega_0})^2}{1 + (\frac{\omega}{\omega_0})^2}}, \quad \tan\theta_\mu = \frac{(\mu_{dc} - \mu_0)\frac{\omega}{\omega_0}}{\mu_{dc} + \mu_0(\frac{\omega}{\omega_0})^2} \tag{57}$$

The frequency-dependent permeability angle has a local maximum ($d\theta_\mu/d\omega = 0$) at the frequency $\omega' = \omega_0\sqrt{\mu_{dc}/\mu_0}$ $\approx$ 80kHz, for which we find:

$$\mu_w(\omega') = \sqrt{\mu_{dc}\mu_0}\, e^{-j\arctan\left(\frac{1}{2}\sqrt{\mu_{dc}/\mu_0}\right)} \approx 16\mu_0 e^{-j82°} \tag{58}$$

The minimum values of θ_0, θ_w, and X_w, at $f = 80$ kHz, observed in Figs 6 and 7, are clearly a consequence of the stationarity point in the complex permeability.

The axial wave parameters, propagation constant and characteristic impedance, are represented against frequency in Fig. 8. Note that the parameters α and β in Fig. 8a are interrelated with R_c and X_c in Fig. 8b via (21). For very low frequencies, α and β are similar in magnitude, so are R_c and X_c. For high frequencies β dominates α, and R_c dominates X_c.

Finally, we pay attention to the pul parameters C_0 and L_0 calculated using the TEM approach (T), the circuit approach (C), and the energy approach (E). Computation results are shown in Fig. 9, the normalized capacitance in Fig. 9a, the normalized inductance in Fig. 9b. Results obtained are much like those for the nonmagnetic wire in Subsection VI-A.

The curves obtained using the T, C and E approaches overlap significantly, differing little among them, the only exception being the inductance for the T-approach, which displays a non-physical trend, increasing from negative real values (at extremely low frequencies) up to 'normal' positive values (at 1 kHz) when it merges with the C and E curves.

Along nine frequency decades the capacitance is seen to increase only by a factor of 3, the inductance decreases by the same factor, and their product L_0C_0 remains practically invariant —this behavior is justified in (52).

The ups and downs observed in the pul skin effect impedance (Fig. 6) seem to have no visible impact on C_0 and L_0, exception to the curves of their imaginary parts (circuit approach), however, the latter not only lack physical meaning but also have very small magnitude compared to the corresponding real parts.

VII. CONCLUSION

This work, devoted to the single-wire transmission line at low frequencies, was mainly focused on the critical analysis, interpretation, computation, and discussion of its per unit length constitutive parameters, namely, the internal pul skin effect impedance, and the external pul capacitance and inductance, C_0 and L_0.

The evaluation of the internal pul skin effect impedance raises no difficulties, practical or conceptual; it can be dealt with the help of the familiar skin effect theory. Nonetheless, we paid particular attention to that topic when addressing the case of magnetic wires (like steel) where the magnetic permeability can be modeled using a complex frequency-domain Debye approach, which, we showed can produce intense fluctuations in the skin effect impedance angle, from 0 to 45°, back to 0, and again up to 45° —an abnormal behavior not possible in nonmagnetic wires. Knowledge of the internal skin effect impedance is crucial for the determination of the properties of the radial wave and of the axial wave guided by the single wire, be it nonmagnetic or magnetic. The link between the skin effect impedance and the wave propagation parameters was established, analyzed, and an approximation was proposed, later confirmed numerically.

Contrarily, the calculation of the external pul inductance and capacitance of the SWTL raises difficulties, practical and conceptual. Those concepts belong with quasi-TEM transmission line theory with two or more wires; their usage

outside such scope is questionable. For example, the E-field lines in the SWTL begin and end at the wire itself —the meaning of capacitance defined between a wire and itself is perplexing, at least. Nevertheless, the literature on SWTL has been accumulating an increasing number of references to pul constitutive parameters; this made us conduct a thorough research on the subject. For that purpose, we considered, analyzed, and compared three approaches with different physical supports: the TEM-approach, the circuit-approach, and the energy-approach. The first mimics ordinary TL analysis, extracting the constitutive parameters from wave parameters. The second makes use of the quasi-static definitions of capacitance and inductance using the familiar ratios charge/voltage and flux/current. The third determines the constitutive parameters from the energy stored in the electromagnetic field around the wire.

The analytical solutions we derived for C_0 and L_0 using the various approaches do not coincide, as their graphical representations also show. Two problems were identified: the TEM-approach leads to negative inductance values at extremely low frequencies; the circuit-approach leads to small but non-zero imaginary parts in the pul inductance and capacitance. The energy-based approach has no physical drawbacks.

Excluding the above identified problems, considering the nine-decade frequency window from 1 Hz to 1 GHz, we concluded that the results of the TEM-approach and circuit-approach converge to the results of the energy-approach, with minor differences of second-order importance. The three approaches provide a common frequency-dependent dominant term for C_0 and, also, for L_0, whose product is $1/c^2$. These pul parameters are, approximately, the same as those of an equivalent coaxial cable with an outer radius equal to the inverse of the absolute value of the radial propagation constant.

APPENDIX A
CONSIDERATIONS ON THE SKIN EFFECT

A legacy of J. C. Maxwell [31], the subject of skin effect is a well-known classical topic in electrical engineering and electromagnetics that has been studied for over a century, from circular cylindrical wires to conductors with more complicated cross-sections.

The body of literature on skin effect analysis is vast; it would require and deserve a whole review article to cover just the major contributions to the field. That is not the purpose of the present article, where the skin effect is a tool, not a target. Nonetheless, with respect to recent advances (2010's) regarding solid and tubular circular geometries, we may cite: [32], [33] for contributions to full time-domain skin-effect theory in homogeneous solid wires; [34], [35] for contributions to accurate numerical computations of skin-effect impedance in homogeneous cylindrical conductors; [36], [37], [38] for contributions to frequency-domain skin-effect impedance and field calculations in inhomogeneous cylindrical structures; and, also, [39], [40] for contributions to the problematics of the solitary conductor.

Although skin-effect analysis is not a target in this work, we take the opportunity to clarify the role of the pul skin-effect impedance Z_w in surface wave context.

In ordinary frequency-domain skin-effect analysis, the sinusoidal current in the solitary circular wire and associated fields are considered z-independent; div and rot Maxwell equations include only radial derivatives, $\partial/\partial z$ derivatives are absent, so are E_r field components. In this context Z_w is calculated using the well-known ordinary skin-effect formula

$$Z_w = \frac{g_w}{2\pi a\sigma_w}\frac{J_0(g_w a)}{J_1(g_w a)}, \quad g_w = \sqrt{-j\omega\mu_w\sigma_w} \tag{A1}$$

However, in surface wave theory, the solitary wire sinusoidal current is not z-independent —see (1). Fields propagate with $e^{-\gamma z}$ and radial **E**-field components are present —see (2)-(4). In this context Z_w is calculated using (A1) but with g_w defined differently, from (6),

$$(Z_w)_{exact} = \frac{g_w}{2\pi a\sigma_w}\frac{J_0(g_w a)}{J_1(g_w a)}, \quad g_w = \sqrt{\gamma^2 - j\omega\mu_w\sigma_w} \tag{A2}$$

Therefore, the pul skin-effect impedances Z_w calculated from surface-wave theory or from ordinary skin-effect theory are, strictly speaking, unequal. However, from an engineering viewpoint, the differences are so small that they can be safely ignored. In fact, the quantity γ^2 appearing in (A2) is of the same order of magnitude of β_0^2 and the latter is many orders of magnitude smaller than $\omega\sigma_w\mu_w$.

Making $\gamma \approx j\beta_0$ (for estimation purposes) yields:

$$\frac{(g_w)_{exact}}{g_w} = \sqrt{1 + \frac{j\gamma^2}{\omega\mu_w\sigma_w}} \approx 1 - j\frac{1}{2}\left(\frac{\mu_0}{\mu_w}\right)\underbrace{\left(\frac{\omega\varepsilon_0}{\sigma_w}\right)}_{\ll 1} \approx 1 \tag{A3}$$

where the inequality $\omega\varepsilon_0 \ll \sigma$ is valid up to the optical range for the case of good conductors. For example, for a copper wire, at 1 GHz, we find $(g_w)_{exact}/g_w \approx 1 - j\frac{1}{2}10^{-9}$—an error smaller than 1 part in a billion. Figure A1 depicts the real and imaginary parts of the pul skin-effect impedance Z_w against frequency, computed using (A1) and (A2), for a copper wire with $a = 1$ mm. No kind of disagreement is observable.

In conclusion:

The general field equations that govern surface wave phenomena collapse in ordinary skin-effect field equations in the limit $\gamma \to 0$, for $r \leq a$.

Albeit different, the results in (A1) and (A2) produce undistinguishable numerical results.

The procedure proposed in this paper, where Z_w from (A1) is plugged in the transcendental equation (22) and the latter is solved for the radial and axial propagation constants, g_0 and γ, permits a complete accurate description of the properties of the Sommerfeld wave.

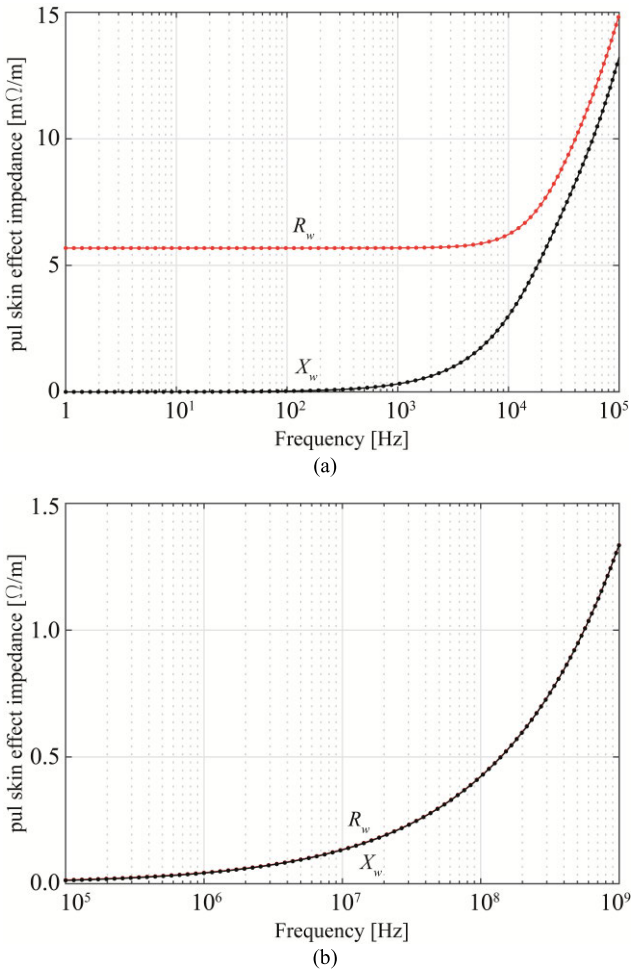

FIGURE 10. Real and imaginary parts of the pul skin effect impedance of a copper wire with radius 1 mm against frequency. Solid lines are exact results from (A2); superimposed circles are approximate results from (A1). (a) f < 0.1 MHz; (b) f > 0.1 MHz.

APPENDIX B
RADIAL INTEGRATION OF $|H|^2$

According to (18), the determination of the characteristic impedance Z_c requires the calculation of the following integral:

$$Int(r) = \int \left(H_1^{(1)}(g_0 r)\right)\left(H_1^{(1)}(g_0 r)\right)^* rdr \tag{B1}$$

where $g_0 = a_0 + jb_0$ is a complex of the 1st quadrant.

Since $(H_n^{(1)}(x))^* = H_n^{(2)}(x^*)$, for $n = 1$ we rewrite (B1) as

$$Int(r) = \int \left(H_1^{(1)}(g_0 r)\right)\left(H_1^{(2)}(g_0^* r)\right) rdr \tag{B2}$$

An identity from the theory of Bessel functions [41], [42], of arbitrary order n, is now useful:

$$\int P_n(pr)Q_n(qr)rdr = \frac{(qr)P_n(pr)\,Q_{n-1}(qr) - (pr)P_{n-1}(pr)\,Q_n(qr)}{p^2 - q^2} \tag{B3}$$

where P_n and Q_n are Bessel functions ($J_n, N_n, H_n^{(1)}$or $H_n^{(2)}$).

By making $p = g_0$, $q = p*$, $P_n = H_1^{(1)}$ and $Q_n = H_1^{(2)}$ in (B3), transforms (B2) into

$$\begin{aligned} Int(r) &= \frac{(g_0^* r)H_1^{(1)}(g_0 r)H_0^{(2)}(g_0^* r) - (g_0 r)H_0^{(1)}(g_0 r)H_1^{(2)}(g_0^* r)}{g_0^2 - (g_0^2)^*} \\ &= \frac{\left((g_0 r)H_0^{(1)}(g_0 r)H_1^{(2)}(g_0^* r)\right)^* - \left((g_0 r)H_0^{(1)}(g_0 r)H_1^{(2)}(g_0^* r)\right)}{4ja_0 b_0} \\ &= -\frac{1}{2a_0 b_0}\mathrm{Im}\left((g_0 r)\,H_0^{(1)}(g_0 r)\,H_1^{(2)}(g_0^* r)\right) \\ &= -\frac{1}{2a_0 b_0}\mathrm{Im}\left((g_0 r)\,H_0^{(1)}(g_0 r)\,(H_1^{(1)}(g_0 r))^*\right) \end{aligned} \tag{B4}$$

To obtain Z_c we need to evaluate $Int(\infty) - Int(a)$. The value of $Int(\infty)$ is found from the asymptotic behavior of the product of the Hankel functions in (B4). Abbreviating $g_0 r = x$, and recalling that $\mathrm{Im}(g_0) = b_0 > 0$ we find

$$\text{For } r \to \infty : x\left(H_0^{(1)}(x)\right)\left(H_1^{(1)}(x)\right)^* \propto \frac{g_0}{|g_0|}e^{-2b_0 r} \to 0$$

In conclusion,

$$\begin{aligned} Z_c &= \frac{\gamma}{2\pi a^2 j\omega\varepsilon_0}\cdot\frac{-Int(a)}{\left|H_1^{(1)}(g_0 a)\right|^2} \\ &= \frac{\gamma}{4\pi a j\omega\varepsilon_0}\mathrm{Im}\left(\frac{g_0}{a_0 b_0}\cdot\frac{H_0^{(1)}(g_0 a)}{H_1^{(1)}(g_0 a)}\right) \end{aligned} \tag{B5}$$

which finally proves (19).

APPENDIX C
RADIAL INTEGRATION OF $|E_z|^2$

According to (37) and (10), the determination of W_z requires the calculation of the following integral:

$$Int'(r) = \int \left(H_0^{(1)}(g_0 r)\right)\left(H_0^{(1)}(g_0 r)\right)^* rdr \tag{C1}$$

Since $(H_n^{(1)}(x))^* = H_n^{(2)}(x^*)$, for $n = 0$ we rewrite (C1) as

$$Int'(r) = \int \left(H_0^{(1)}(g_0 r)\right)\left(H_0^{(2)}(g_0^* r)\right) rdr \tag{C2}$$

Using the identity in (B3), with $p = g_0$, $q = p*$, $P_n = H_0^{(1)}$ and $Q_n = H_0^{(2)}$, transforms (C2) into

$$Int'(r) = \frac{(g_0^* r)H_0^{(1)}(g_0 r)H_{-1}^{(2)}(g_0^* r) - (g_0 r)H_{-1}^{(1)}(g_0 r)H_0^{(2)}(g_0^* r)}{g_0^2 - (g_0^2)^*}$$

which, taking into account that $H_{-1}^{(n)} = -H_1^{(n)}$, yields

$$\begin{aligned} Int'(r) &= \frac{(g_0 r)H_1^{(1)}(g_0 r)H_0^{(2)}(g_0^* r) - (g_0^* r)H_0^{(1)}(g_0 r)H_1^{(2)}(g_0^* r)}{g_0^2 - (g_0^2)^*} \\ &= \frac{\left((g_0^* r)H_0^{(1)}(g_0 r)H_1^{(2)}(g_0^* r)\right)^* - \left((g_0^* r)H_0^{(1)}(g_0 r)H_1^{(2)}(g_0^* r)\right)}{4ja_0 b_0} \end{aligned}$$

$$= -\frac{1}{2a_0b_0}\mathrm{Im}\left((g_0^*r)H_0^{(1)}(g_0r)H_1^{(2)}(g_0^*r)\right)$$
$$= -\frac{1}{2a_0b_0}\mathrm{Im}\left((g_0^*r)H_0^{(1)}(g_0r)\,(H_1^{(1)}(g_0r))^*\right) \quad \text{(C3)}$$

Noting again that $Int'(\infty) = 0$, the contribution W_z for the electric energy in (37) takes the form:

$$W_z = \frac{|g_0^2|\,I_{rms}^2}{4\pi a^2\omega^2\varepsilon_0}\cdot\frac{-Int'(a)}{\left|H_1^{(1)}(g_0a)\right|^2}$$
$$= \frac{|g_0^2|\,I_{rms}^2}{8\pi a\omega^2\varepsilon_0}\mathrm{Im}\left(\frac{g_0^*}{a_0b_0}\cdot\frac{H_0^{(1)}(g_0a)}{H_1^{(1)}(g_0a)}\right) \quad \text{(C4)}$$

Further, eliminating the Hankel functions from (17), and making $a_0b_0 = \alpha\beta$, we find

$$W_z = \mathrm{Re}\left(\frac{g_0^2}{2\alpha\beta}Z_w^*\right)\frac{I_{rms}^2}{2\omega} \quad \text{(C5)}$$

which finally proves (39).

REFERENCES

[1] A. Sommerfeld, "Ueber die fortpflanzung elektrodynamischer wellen langs eines drahtes," *Ann. Phys.*, vol. 303, no. 2, pp. 233–290, 1899.
[2] R. Warnock, "On the propagation of electrodynamic waves along a wire by A. Sommerfeld," *Electromagnetics*, vol. 39, no. 5, pp. 281–324, Jul. 2019.
[3] J. Zenneck, "Uber die fortpflanzung ebener elektromagnetischer wellen langs einer ebenen leiterflache und ihre beziehung zur drahtlosen telegraphie," *Ann. Phys.*, vol. 328, no. 10, pp. 846–866, 1907.
[4] G. Goubau, "Surface waves and their application to transmission lines," *J. Appl. Phys.*, vol. 21, no. 11, pp. 1119–1128, Nov. 1950.
[5] G. Goubau, "Single-conductor surface-wave transmission lines," *Proc. IRE*, vol. 39, no. 6, pp. 619–624, Jun. 1951.
[6] G. Goubau, "On the excitation of surface waves," *Proc. IRE*, vol. 40, no. 7, pp. 865–868, Jul. 1952.
[7] S. J. Orfanidis, "Surface waveguides," in *Electromagnetic Waves and Antennas*. Piscataway, NJ, USA: Rutgers, 2016, ch. 10. [Online]. Available: https://www.ece.rutgers.edu/orfanidi/ewa
[8] S. A. Maier, *Plasmonics: Fundamentals and Applications*. New York, NY, USA: Springer, 2007.
[9] G. E. Elmore, "Single conductor surface wave transmission line system for terminating E-field lines at points along the single conductor," Patent U.S. 8 497 749 B2, Jul. 30, 2013.
[10] S. Galli, J. Liu, and G. Zhang, "Bare metal wires as open waveguides, with applications to 5G," in *Proc. IEEE Int. Conf. Commun. (ICC)*, May 2018, pp. 1–6.
[11] D. Molnar, T. Schaich, A. Al-Rawi, and M. Payne, "Interaction between surface waves on wire lines," *Proc. Roy. Soc. A, Math., Phys. Eng. Sci.*, vol. 477, no. 2246, Feb. 2021, Art. no. 20200795.
[12] T. Schaich, D. Molnar, A. Al Rawi, and M. Payne, "Surface wave transmission line theory for single and many wire systems," *J. Appl. Phys.*, vol. 130, no. 19, Nov. 2021, Art. no. 194902.
[13] T. Schaich, E. Dinc, D. Molnar, M. Drolia, S. Bukhari, A. Aziz, I. Toledano, T. Morsman, F. Burton, M. Crisp, E. de Lera Acedo, A. A. Rawi, R. Penty, and M. Payne, "Advanced modeling of surface waves on twisted pair cables: Surface wave stopbands," *IEEE Trans. Microw. Theory Techn.*, vol. 70, no. 5, pp. 2541–2552, May 2022.
[14] T. Schaich, "Modelling of electromagnetic surface wave propagation for high-speed communications," Ph.D. dissertation, Fac. Phys. Chem., Univ. Cambridge, Cambridge, U.K., 2022.
[15] B. J. Vaughn, D. Peroulis, and A. Fisher, "Mid-range wireless power transfer based on Goubau lines," in *IEEE MTT-S Int. Microw. Symp. Dig.*, Philadelphia, PA, USA, Jun. 2018, pp. 968–971.
[16] B. J. Vaughn, A. Fisher, and D. Peroulis, "Electrically-coupled Goubau-line-based wireless power transfer system," *IEEE Access*, vol. 7, pp. 115886–115900, 2019.
[17] A. Ametani, Y. Miyamoto, Y. Baba, and N. Nagaoka, "Wave propagation on an overhead multiconductor in a high-frequency region," *IEEE Trans. Electromagn. Compat.*, vol. 56, no. 6, pp. 1638–1648, Dec. 2014.
[18] E. Stracqualursi, R. Araneo, J. B. Faria, P. Burghignoli, and A. Andreotti, "The Sommerfeld–Goubau theory for the transient response of towers," in *Proc. 20th Int. Conf. Harmon. Quality Power (ICHQP)*, Naples, Italy, May 2022, pp. 1–5.
[19] E. Stracqualursi, R. Araneo, J. B. Faria, P. Burghignoli, A. Andreotti, and B. Kordi, "On the transient analysis of towers: A revised theory based on Sommerfeld–Goubau wave," *IEEE Trans. Power Del.*, vol. 38, no. 1, pp. 309–318, Feb. 2023.
[20] R. Holland and R. H. St. John, "EM pickup and scattering by a wire," *IEEE Trans. Electromagn. Compat.*, vol. 42, no. 4, pp. 461–469, Nov. 2000.
[21] U. Paoletti, T. Suga, and H. Osaka, "Equivalent circuit for Sommerfeld wave," *IEICE Electron. Exp.*, vol. 8, no. 19, pp. 1590–1595, 2011.
[22] B. Vaughn and D. Peroulis, "An updated applied formulation for the Goubau transmission line," *J. Appl. Phys.*, vol. 126, no. 19, Nov. 2019, Art. no. 194902.
[23] J. B. Faria, *Electromagnetic Foundations of Electrical Engineering*. Chichester, U.K.: Wiley, 2008.
[24] J. B. Faria, *Multiconductor Transmission-Line Structures: Modal Analysis Techniques*. New York, NY, USA: Wiley, 1993.
[25] J. B. Faria, "Comments on surface wave transmission line theory for single and many wire systems," *J. Appl. Phys.*, vol. 131, no. 24, 2022, Art. no. 246101.
[26] T. Schaich, D. Molnar, A. Al Rawi, and M. Payne, "Response to comment on surface wave transmission line theory for single and many wire systems," *J. Appl. Phys.*, vol. 131, no. 24, 2022, Art. no. 246102.
[27] J. Polo Jr. and A. Lakhtakia, "Surface electromagnetic waves: A review," *Laser Photon. Rev.*, vol. 5, no. 2, pp. 234–246, Mar. 2011.
[28] C. V. Topping and S. J. Blundell, "A.C. susceptibility as a probe of low-frequency magnetic dynamics," *J. Phys., Condens. Matter*, vol. 31, no. 1, Jan. 2019, Art. no. 013001.
[29] N. Bowler, "Frequency-dependence of relative permeability in steel," in *Proc. AIP Conf.*, 2006, pp. 1269–1276.
[30] J. L. Snoek, "Dispersion and absorption in magnetic ferrites at frequencies above one Mc/s," *Physica*, vol. 14, no. 4, pp. 207–217, May 1948.
[31] J. C. Maxwell, *A Treatise on Electricity and Magnetism*. Oxford, U.K.: Oxford Univ. Press, 1892.
[32] J. B. Faria and M. S. Raven, "On the success of electromagnetic analytical approaches to full time-domain formulation of skin effect phenomena," *Prog. Electromagn. Res. M*, vol. 31, pp. 2145–2154, 2013.
[33] M. S. Raven, "Skin effect in the time and frequency domain—Comparison of power series and Bessel function solutions," *J. Phys. Commun.*, vol. 2, no. 3, Mar. 2018, Art. no. 035028.
[34] D. Lovric, V. Boras, and S. Vujevic, "Accuracy of approximate formulas for internal impedance of tubular cylindrical conductors for large parameters," *Prog. Electromag. Res. M*, vol. 16, pp. 171–184, 2011.
[35] S. Vujevic, D. Lovric, and V. Boras, "High-accurate numerical computation of internal impedance of cylindrical conductors for complex arguments of arbitrary magnitude," *IEEE Trans. Electromagn. Compat.*, vol. 56, no. 6, pp. 1431–1438, Dec. 2014.
[36] J. A. M. Brandao Faria, "A matrix approach for the evaluation of the internal impedance of multilayered cylindrical structures," *Prog. Electromagn. Res. B*, vol. 28, pp. 351–367, 2011.
[37] J. A. M. B. Faria, "Skin effect in inhomogeneous Euler–Cauchy tubular conductors," *Prog. Electromagn. Res. M*, vol. 18, pp. 89–101, 2011.
[38] J. Acero, C. Carretero, I. Lope, R. Alonso, and J. M. Burdío, "Analytical solution of the induced currents in multilayer cylindrical conductors under external electromagnetic sources," *Appl. Math. Model.*, vol. 40, nos. 23–24, pp. 10667–10678, Dec. 2016.
[39] O. Coufal, "Comments on skin effect in solitary solid tubular conductor," *Adv. Math. Phys.*, vol. 2011, Jan. 2011, Art. no. 983678.
[40] O. Coufal, "On inductance and resistance of solitary long solid conductor," *Acta Technica*, vol. 57, no. 1, pp. 75–89, 2012.
[41] G. N. Watson, *A Treatise in the Theory of Bessel Functions*, 2nd ed. Cambridge, U.K.: Cambridge Univ. Press, 1958.
[42] F. W. J. Olver, D. W. Lozier, R. F. Boisvert, and C. W. Clark, *NIST Handbook of Mathematical Functions*. Cambridge, U.K.: Cambridge Univ. Press, 2010.

JOSÉ A. BRANDÃO FARIA (Life Fellow, IEEE) was born in Figueira da Foz, Portugal, in 1952. He received the Ph.D. and Habilitation degrees in electrical engineering from Instituto Superior Técnico (IST), School of Engineering, University of Lisbon, Lisbon, Portugal, in 1986 and 1992, respectively. Retired in 2022, he has been a Full Professor of electrical engineering with IST, since 1994, where he taught courses on electromagnetics and circuit analysis theory. Currently, his research activities are carried out with Instituto de Telecomunicações, Lisbon, where he leads the Applied Electromagnetics Group. He is the author of four books on electrical engineering subjects: *Análise de Circuitos* (Portugal, IST Press, 2019), *Electromagnetic Foundations of Electrical Engineering* (U.K., Wiley, 2008), *Óptica* (Portugal, Ed. Presença, 1995), and *Multiconductor Transmission-Line Structures* (USA, Wiley, 1993). He has authored over 130 scientific articles in main peer-reviewed periodicals. His research interests include electromagnetic-field problems, applied electromagnetics, wave propagation phenomena in multiconductor transmission lines, and overhead power lines. In 2016, he was a recipient of the Scientific Prize in Electrical Engineering Research awarded by the University of Lisbon.

RODOLFO ARANEO (Senior Member, IEEE) received the M.S. (summa cum laude) and Ph.D. degrees in electrical engineering from University of Rome ''La Sapienza'', Rome, Italy, in 1999 and 2002, respectively. In 1999, he was a Visiting Student with the National Institute of Standards and Technology, Boulder, CO, USA, where he was engaged in TEM cells and shielding. In 2000, he was a Visiting Researcher with the Department of Electrical and Computer Engineering, University of Missouri–Rolla, Rolla, MO, USA, where he was engaged in printed circuit boards and finite-difference time-domain techniques. He is currently a Full Professor with Department of Astronautical, Electrical and Energy Engineering, University of Rome ''La Sapienza''. He has authored more than 220 papers in international journals and conference proceedings. He is the coauthor of the book *Electromagnetic Shielding* (IEEE Wiley, 2008) and *Electrical Safety Engineering of Renewable Energy Systems* (IEEE Wiley, 2021). His research interests include electromagnetic compatibility, energy harvesting, and piezotronics based on piezoelectric ZnO nanostructures, graphene electrodynamics, the development of numerical and analytical techniques for modeling high-speed printed circuit boards, shielding, transmission lines, periodic structures, and devices based on graphene. In 2018, he was nominated as a fellow of the Applied Computational Electromagnetics Society. In 1999, he was a recipient of the Past President's Memorial Award from the IEEE Electromagnetic Compatibility Society. Since 2015, he has been the General Chair of the IEEE International Conference on Environment and Electrical Engineering.

ERIKA STRACQUALURSI (Member, IEEE) received the M.S. (summa cum laude) and Ph.D. degrees in electrical engineering from University of Rome ''La Sapienza'', Rome, Italy, in 2019 and 2023, respectively. In 2021, she was a Visiting Ph.D. Student with the High Voltage Laboratory, Aristotle University of Thessaloniki, Thessaloniki, Greece, where she was involved in studies of corona discharge along transmission lines and grounding. She is currently a Research Fellow in electrical engineering with the Department of Astronautical, Electrical and Energy Engineering, University of Rome ''La Sapienza''. Her research interests include finite-difference time-domain methods, and transmission line analysis and modeling.